

Accelerating MCMC with Quantum Walks: Design, Implementation, and Results

Aingeru Ramos^{1*}, Jose A. Pascual^{2†} and Javier Navaridas^{2†}

^{1*}Basque Center for Materials, Applications and Nanostructures (BCMaterials), Martina Casiano building. EHU Technology Park., Leioa, 48940, Spain.

²Dept. of Computer Architecture and Technology, University of the Basque Country (UPV/EHU), Manuel Lardizabal Pasalekua, San Sebastián, 20018, Spain.

*Corresponding author(s). E-mail(s): aingeru.ramos@bcmaterials.net;
Contributing authors: joseantonio.pascual@ehu.eus;
javier.navaridas@ehu.eus;

†These authors contributed equally to this work.

Abstract

Markov Chain Monte Carlo (MCMC) methods are algorithms for sampling probability distributions, often applied to the Boltzmann distribution in physical and chemical models, such as protein folding and the Ising model. These methods enable the study of such systems by sampling their most probable states. However, sampling multidimensional and multimodal distributions with MCMC demands significant computational resources, leading to the development of techniques aimed at improving sampling efficiency. In this context, quantum computing, with its potential to accelerate classical methods, emerges as a promising solution to the sampling problem. In this work, we present the design and implementation of a novel MCMC algorithm (QMCMC) based on the Discrete Quantum Walk (DQW) algorithm. We test several Gaussian distributions, including mixtures and demonstrate that it effectively captures the structure of the target distribution by leveraging quantum superposition. In addition, we introduce a circuit extension that significantly improves convergence speed, which in turn enhances the scalability of the algorithm.

Keywords: Markov Chain Monte Carlo, Quantum Computing, Algorithm Design.

1 Introduction

The study of physical systems requires solving equations derived from the natural laws that govern them, often an intractable task due to (i) the lack of a closed-form solution, or (ii) the complexity of the equations, which prevents manual resolution [1]. Because of that, the use of computational methods has become fundamental in physics, and in general, across all scientific disciplines. The use of such methods dates back to the 20th century and marks the birth of computational physics and its most fundamental tool: the simulation of physical models.

These simulations can be broadly divided into two categories. The first one encompasses physical simulations, which create a virtual version of the system under study and emulate the physical laws governing its evolution. These simulations require significant computational resources and provide approximate solutions using numerical and statistical methods. This enables the extraction of macroscopic characteristics such as pressure, temperature, or density, parameters relevant for analyzing and understanding the system under study. In this context, Markov Chain Monte Carlo (MCMC) methods have become widely used. The first algorithm developed in this family of methods was the Metropolis-Hastings (MH) algorithm, based on the works of Metropolis [2] and Hastings [3], which defines the general scheme of all MCMC processes. These algorithms, capable of sampling any given probability distribution, are commonly used in physical-chemical simulations together with the Boltzmann distribution which describes the probability of a system being in a particular state. As a result, sampling the Boltzmann distribution through MCMC methods enables exploration of the system's state space and, yields samples of its most probable states. However, in real systems, with immense and often multidimensional state spaces, the effectiveness of these methods decreases, often resulting in non-representative samples of the target distribution. Various techniques have been developed to accelerate convergence, but all of them, in one way or another, demand a substantial increase in computational resources.

Quantum computing is an emerging field that explores the use of principles from quantum mechanics to perform computation [4]. Unlike classical computers, quantum computers encode information in qubits, which can represent multiple states simultaneously, enabling calculations across all those states at once. This unique property, inherent to quantum mechanics, promises **exponential acceleration** of certain algorithms, offering great potential in applications that require huge computational resources, such as molecular simulation, artificial intelligence, and optimization. However, quantum computing still faces significant technical challenges, such as quantum error correction and the stability of qubits in superposition [5]. Despite these obstacles, the immense potential of the technology continues to drive advancements in both algorithm design and quantum hardware development.

In this paper, we aim to develop a quantum implementation of the MCMC algorithm by designing a quantum circuit based entirely on the Discrete Quantum Walk (DQW) scheme. We refer to this circuit as Quantum MCMC, or simply QMCMC. We present the circuit, explain its design, and analyze the resulting distributions. The first results indicate that the algorithm is capable of converging toward the target

distribution, although its convergence rate remains too slow for practical use in real-world problems with the base implementation. To boost the convergence speed, we propose a modification of the proposed circuit that allows to increase the number of movements evaluated in each iteration.

1.1 Related Work

The concept of Quantum Walk (QW) was introduced by Aharonov and his collaborators in 1993 [6], proposing a quantum version of classical random walks. Unlike its classical counterpart, which moves randomly through a set of positions, the quantum walker can explore multiple paths simultaneously by leveraging quantum superposition. This property allows for faster and more efficient exploration of the state space. This proposal proved crucial for the development of quantum computing, as it demonstrated how quantum stochastic processes, taking advantage of the quadratic acceleration due to superposition, could outperform classical methods.

In 2003, Ambainis, in a work later published in 2007 [7], made a key breakthrough by demonstrating that QWs could accelerate search algorithms in one-dimensional spaces. Unlike classical methods, which traverse space linearly, a quantum walker can locate information much faster, significantly reducing search time. This result highlighted the potential of QWs as powerful tools for efficiently exploring large spaces, by leveraging the superposition of paths guiding the search process.

Building on the work of Aharonov and Ambainis, Szegedy [8] generalized QWs to multidimensional spaces in 2004, enabling their application to graphs and more complex structures. This advancement opened new possibilities for designing quantum algorithms in higher dimensions. Notable examples include Childs' work [9] on improving quantum search in high-dimensional complex graphs, and Ambainis' [10] use of QWs in hypercubes, which improved efficiency in optimization and search problem involving highly symmetric structures.

In 2009, Child [11] showed that QWs are not only useful for accelerating search algorithms, but can also have the potential to be adapted for universal quantum computation. This discovery significantly expanded their application, extending beyond search tasks to the simulation of complex quantum systems and the development of more general-purpose quantum algorithms. Since the pioneering work of Aharonov, Ambainis, and Szegedy, research on QWs has evolved in multiple directions. Their demonstrated ability to accelerate search algorithms and simulate complex quantum systems has led to applications in quantum optimization, physical and chemical simulations, and universal algorithms design [12–14].

The QW algorithm is an iterative algorithm which explores the state space more efficiently than its classical counterpart, generating a distribution that benefits from the superposition. However, despite offering some control over the output distribution, this control remains limited. In this context, the aim of our work is to extend that level of control, enabling the quantum walk to approximate arbitrary distributions more effectively. This evolution brings the method closer to a fully quantum version of the MCMC algorithm.

2 Theoretical Framework

2.1 Markov Chain Monte Carlo

Let X be a random variable that follows a probability distribution $f(x)$, and consider a random sample $\{X_0, X_1, X_2, \dots, X_n\}$ of size $n + 1$, where the frequency of each value of X is proportional to the probability given by f . While some distributions have well-known direct sampling methods, these are rare. In most cases, approximation methods are required, such as **Monte Carlo methods**, which provide independent samples from the distribution. In contrast, MCMC methods also sample from any target distribution f , but the resulting samples are dependent, forming a chain constructed by the Markov process.

The basic scheme of the Metropolis-Hastings algorithm is as follows. Let x be a variable initialized with a random value x_{init} . For each of the N iterations, the algorithm performs three steps: (i) a candidate trial x_{trial} is generated using a generator function g such that $x_{trial} = g(x)$, (ii) the acceptance probability for the new state is computed using the acceptance function A , as shown in Equation (1), and (iii) the current value of x is either replaced by x_{trial} according to the previous acceptance probability, or kept and stored in a list. After N iterations, the list contains a Markov chain that approximates the target distribution f .

$$A(x_{trial}, x) = \min\left(1, \frac{f(x_{trial})}{f(x)}\right) \quad (1)$$

All algorithms in the MCMC family follow this basic scheme, with slight variations in the proposal or acceptance functions. However, they must preserve ergodicity, a key property that ensures, given enough iterations, the algorithm can reach all possible states of the target distribution f . This property depends on the design of the proposal function g , the acceptance function A , and the distribution f itself. When ergodicity holds, the process is guaranteed to eventually explore the entire support of the distribution as $N \rightarrow \infty$, producing statistically representative samples (see Figure 1).

Despite their utility, MCMC algorithms face a significant limitation: slow convergence, particularly when the distribution f is multimodal, high-dimensional, or defined over a large or intractable state space. In such cases, the number of iterations required to obtain representative samples can be prohibitively large, making the algorithm impractical in its basic form. Although many improved variants[15][16][17] and convergence-acceleration techniques have been proposed, the challenge of efficient and scalable sampling remains an open research problem.

2.2 Discrete Quantum Walk

2.2.1 Quantum States and Gates

The state of a quantum system is described by a column vector $|\psi\rangle$ in a Hilbert space \mathcal{H} , which is spanned by a set of orthonormal basis vectors $\{|\phi_0\rangle, |\phi_1\rangle, \dots, |\phi_{n-1}\rangle\}$,

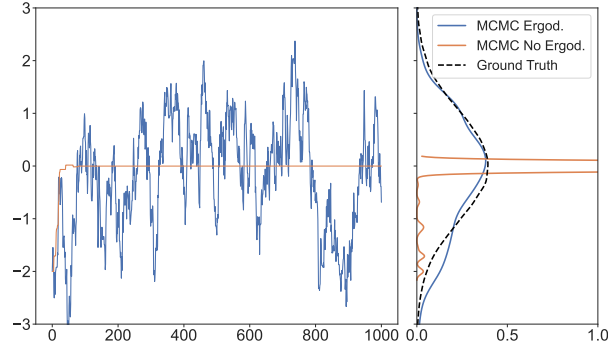


Fig. 1: Left: sample chains generated using different acceptance functions. Right: the resulting distributions for each chain, compared against the true distribution $\mathcal{N}(0, 1)$. The figure illustrates how ergodicity affects convergence to the target distribution.

each in the complex vector space \mathbb{C}^n ¹. In quantum mechanics, the basis states $|\phi_i\rangle$ correspond to measurable, distinguishable outcomes, while a general state $|\psi\rangle$ is a linear combination (superposition) of the basis vectors. The coefficients c_i represent the probability amplitudes of measuring each $|\phi_i\rangle$ state, so they must fulfill the normalization condition. These superposition states are a fundamental feature of quantum systems and form the basis for quantum parallelism.

$$|\psi\rangle = \sum_{i=0}^{|\mathcal{H}|-1} c_i |\phi_i\rangle; \quad \text{where } \sum_{i=0}^{|\mathcal{H}|-1} c_i^2 = 1; \quad c_i \in \mathbb{C}$$

The qubit is the quantum analog of a classical bit. It exists in a two-dimensional Hilbert space \mathcal{H}_2 , spanned by the basis vectors $\{|0\rangle, |1\rangle\}$. Multiple qubits can be combined to form a quantum register (or qregister), whose state resides in the tensor product space $\mathcal{H}_2^{\otimes n} = \mathcal{H}_{2^n}$, where n is the number of qubits. While structurally analogous to classical bit arrays, qubits, and by extension qregisters, can exist in superpositions of all possible states simultaneously. This capability underlies the quantum parallelism that gives quantum computing its potential advantage over classical computation.

To perform computation on a quantum system, it is essential to manipulate the state of a quantum register in a controlled manner. This is done by applying quantum gates, which are unitary operators U that transform an initial state $|\psi_0\rangle$ into another state $|\psi_1\rangle$ according to $U|\psi_0\rangle = |\psi_1\rangle$. A sequence of quantum gates corresponds to a sequence of unitary operations, applied in succession to the register. If U_0, U_1, \dots, U_n are such operations, then the final state is given by the following equation; where U_T represents the total transformation applied to the system.

¹The symbol $\langle\psi|$ represents the transposed conjugate of $|\psi\rangle$ ($\langle\psi| = |\psi\rangle^\dagger$). That is, $\langle\psi|$ is the row vector of the same $|\psi\rangle$ column vector.

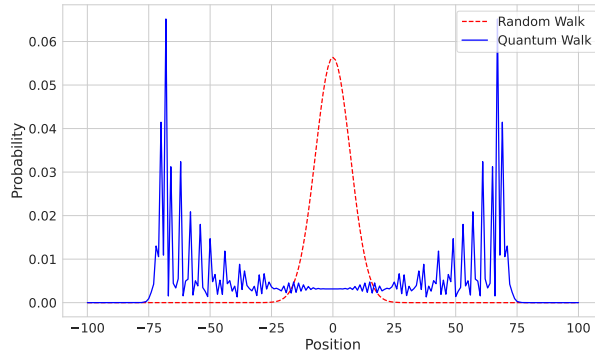


Fig. 2: Comparison of the probability distributions over the state space Σ after 100 iterations of a classical Random Walk (red dashed line) and a Discrete Quantum Walk (blue solid line), both starting from the initial position $x_0 = 0$ with equal probability $p = 0.5$ of moving left or right. The quantum version exhibits faster spatial spread and higher variance than its classical counterpart.

$$U_n \cdots U_1 U_0 |\psi_0\rangle = U_T |\psi_0\rangle = |\psi_{n+1}\rangle$$

2.2.2 Random vs. Quantum Walk

A Random Walk (RW) is an iterative stochastic process in which a walker moves randomly through a space by updating its position over time. These spaces are typically discrete sets of positions $\{x\}$, where $x \in \Sigma$ and Σ represent the domain being explored (e.g., $\Sigma = \mathbb{Z}$ for the one-dimensional case, or $\Sigma = \mathbb{Z} \times \mathbb{Z}$ for two dimensions). The process consists of two key components: (i) a decider which randomly selects an action (a move) from a set \mathcal{A} of allowed moves (depending on the topology of Σ), and (ii) the current position of the walker, which is updated based on the chosen action.

After t iterations, the stochastic nature of the process causes the walker’s position to follow a probability distribution over the positions in Σ . In the one-dimensional case ($\Sigma = \mathbb{Z}$), the actions set is defined as $\mathcal{A} = \{-1, 1\}$, with -1 representing the leftward movement ($x \leftarrow x-1$) and $+1$ the rightward movement ($x \leftarrow x+1$). Assuming the actions are chosen with equal probability and the initial state is $x_0 = 0$, the resulting probability distribution after $t = 100$ iterations is shown in Figure 2 (red dashed line).

The Discrete Quantum Walk (DQW) is the quantum analog of the classical Random Walk, and, like its classical counterpart, it consists of two core components: a position register and a decider (or “coin”) register. These are implemented as quantum registers (qregisters) with associated Hilbert spaces $\mathcal{H}_x = \{|x\rangle\}_{x \in \Sigma}$ for the position and $\mathcal{H}_d = \{|a\rangle\}_{a \in \mathcal{A}}$ for the decider. Together, these registers define the full quantum state of the system. The evolution of the system is driven by a unitary operation U , which applies a single step of the quantum walk. After t iterations, the system evolves from an initial state $|\psi_0\rangle$ to a final state $|\psi_t\rangle = U^t |\psi_0\rangle$.

The operator U can be decomposed into two components: the coin operator C , which generates a superposition of possible actions (from the action set \mathcal{A}) in the decider register, and the shift operator S , which updates the position register based on the selected action. These components are combined according to (2), where I is the identity operator on the position register, and \otimes denotes the tensor product.

$$U = S \cdot (C \otimes I) \quad (2)$$

The coin operator C plays a central role in the behavior of the Discrete Quantum Walk. In the classical Random Walk, the walker's position is updated at each step based on a single action selected by the decision maker from the action set \mathcal{A} . In contrast, the quantum version uses the C operator to place the decider's register into a superposition of all possible actions in \mathcal{A} . This enables the walker to evolve, in a single iteration, as if it were simultaneously following every available path.

To illustrate the behavior of the QW, we again consider the one-dimensional case, $\Sigma = \mathbb{Z}$, as previously done for the classical Random Walk. In this setting, we define the decider's register as $\mathcal{H}_d = \{|H\rangle, |T\rangle\}$, where $|H\rangle$ corresponds to a leftward move ($x \leftarrow x-1$) and $|T\rangle$ to a rightward move ($x \leftarrow x+1$).² In this context, the quantum operators C (coin) and S (shift) take the specific forms given in Equation (3).

Before analyzing the evolution of the walker's distribution in $\Sigma = \mathbb{Z}$, it is helpful to examine the coin operator C . The matrix C defined in Equation (3) represents a general coin operator that creates a superposition of the basis states $|H\rangle$ and $|T\rangle$, modulated by the parameters θ, γ_0 and γ_1 . The parameter θ , often referred to as the rotation angle, determines the weighting of the superposition and lies within the interval $[0, 2\pi)$. For example, when $\theta = \frac{\pi}{4}$, the matrix reduces to a well-known Hadamard operator, which produces an equal (equiprobable) superposition of the two states. Other values of θ introduce a bias, favoring one direction over the other.

The values γ_0 and γ_1 , both within the range $[0, \pi)$, are referred to as the phases of the coin operator. These values influence the global and relative phases of the resulting quantum state, a property that emerges from the fact that quantum states are defined over the complex vector space C^n . Importantly, these phases do not affect the probabilities associated with each basis state in the superposition. As a result, for a given bias (determined by θ), there exists an infinite family of equivalent coin operations that differ only by their phases.

$$C = \cos \theta |H\rangle \langle H| + e^{i\gamma_0} \sin \theta |H\rangle \langle T| + e^{i\gamma_1} \sin \theta |T\rangle \langle H| - e^{i(\gamma_0+\gamma_1)} \cos \theta |T\rangle \langle T| \quad (3)$$

$$S = \sum_{\forall x} |H, x-1\rangle \langle H, x| + \sum_{\forall x} |T, x+1\rangle \langle T, x|$$

²The notation H and T originates from the DQW literature, referencing "Head" and "Tail", the two outcomes of a coin flip, mirroring the role of the decision mechanism.

To analyze the evolution of the system in the one-dimensional case $\Sigma = \mathbb{Z}$, we consider the initial state $|\psi_0\rangle = |H, 0\rangle$ as defined in Equation (4). Applying the unitary operator U to $|\psi_0\rangle$ yields the next state $|\psi_1\rangle$. Recall that the coin operator C creates a superposition over the decider’s basis states, meaning all possible actions are chosen simultaneously. In this case, the walker moves both to the left ($x \leftarrow x - 1$) and to the right ($x \leftarrow x + 1$) at once. As shown in Equation (5), the resulting state reflects this bidirectional evolution, with the amplitude (and thus probability) of each position determined by the action’s contribution in the coin superposition.

Reapplying the operation U to $|\psi_1\rangle$, the system further evolves from each of its current positions ($|H, -1\rangle$ and $|H, +1\rangle$), resulting in the state $|\psi_2\rangle$ given in Equation (6). It is important to observe that the amplitudes of the final states encode the interference of multiple quantum paths. For example, the amplitude at position $|T, 0\rangle$ arises from a path that first moves left from $|H, 0\rangle$ with amplitude $\cos \theta$ followed by a rightward move via the decider’s action $|T\rangle$ with amplitude $e^{i\gamma_1} \sin \theta$. This illustrates how probability amplitudes combine across time steps, resulting in constructive or destructive interference depending on the phases γ_0 and γ_1 .

$$|\psi_0\rangle = |H\rangle |0\rangle = |H, 0\rangle \quad (4)$$

$$|\psi_1\rangle = U |\psi_0\rangle = \cos \theta |H, -1\rangle + e^{i\gamma_1} \sin \theta |T, +1\rangle \quad (5)$$

$$\begin{aligned} |\psi_2\rangle = & \cos^2 \theta |H, -2\rangle + e^{i(\gamma_0 + \gamma_1)} \sin^2 \theta |H, 0\rangle + \\ & e^{i\gamma_1} \sin \theta \cos \theta |T, 0\rangle - e^{i(\gamma_0 + 2\gamma_1)} \sin \theta \cos \theta |T, +2\rangle \end{aligned} \quad (6)$$

Figure 2 compares the probability distribution of the walker in a classical Random Walk (RW, red dashed line) and a Quantum Walk (QW, blue solid line), both evaluated after $t = 100$ iterations from the same initial position $x_0 = 0$. As observed, the QW explores a significantly broader region of the space Σ , reaching positions much farther from the origin compared to the RW under the same number of steps. This reflects the greater dispersion achieved by the quantum process. Analytically, the dispersion (standard deviation) of a classical RW scales as $\mathcal{O}(\sqrt{t})$ whereas for a QW it scales as $\mathcal{O}(t)$, demonstrating a quadratic speedup in spatial exploration. This acceleration arises from the QW’s ability to leverage quantum superposition: the decider register evolves into a superposition of actions, enabling the walker to propagate in multiple directions simultaneously. This behavior is clearly illustrated in the first two steps of the system’s evolution (see Equations (5) and (6)).

3 From Quantum Walk to Quantum MCMC

Despite the promise of the Discrete Quantum Walk algorithm to achieve quadratic acceleration in the exploration state space, as discussed at the end of Subsection 2.2,

the final distribution of the position register $|\psi_t\rangle$ after t iterations is restricted to a specific family of probability distributions. The goal of this work is to develop a quantum version of the Markov Chain Monte Carlo (MCMC) algorithm, referred to as QMCMC, based on the DQW algorithm. To achieve this, we introduce a new register, referred to as the “coin”, which biases the selection of movement directions in the decision process according to the walker’s current position. This directional bias is determined by the acceptance function introduced in Subsection 2.1. As a result, the system behaves like an MCMC process, generating a user-defined target distribution f , which can then be sampled through multiple measurements of the position register, all while preserving the enhanced exploration capabilities provided by the quantum walk.

As outlined in Subsection 2.1, every MCMC process consists of three steps: generating a movement proposal, calculating the probability of accepting the proposed move, and updating the current position if the proposal is accepted. The quantum circuit we propose, shown in Figure 3, is designed to emulate this behavior through four core quantum gates: (i) TRIAL, (ii) DISC, (iii) C GROUP and (iv) SHIFT. Before describing the function of each gate, it is important to clarify the idea behind the design and the specific role of each quantum register involved in the circuit.

The proposed circuit consists of the following quantum registers:

- The action register $|a\rangle$ represents an action from the set \mathcal{A} derived from the state space Σ . Due to quantum superposition, this register can simultaneously encode a distribution over all possible actions, enabling efficient parallel exploration.
- The position register $|x\rangle$ stores the current position of the walker in the space Σ . Similar to $|a\rangle$, it benefits from quantum superposition to represent multiple positions simultaneously.
- The trial register $|t\rangle$ is an auxiliary register used to store the trial state proposed based on the current values of $|a\rangle$ and $|x\rangle$.
- The acceptance register $|\text{acc}\rangle$ encodes the discretized acceptance probability associated with the proposed move. Its value is computed using the DISC gate.
- The coin register $|\text{coin}\rangle$ acts as a quantum decision mechanism, determining whether the proposal will be accepted or rejected, using the probability encoded in $|\text{acc}\rangle$, to modulate the final outcome.

At the start of the circuit’s execution, all the quantum registers are initialized to the state $|0\rangle$, except for the position register $|x\rangle$, which may be initialized to any arbitrary value representing the initial position of the walker. In this case, to avoid the initial position selection problem encountered in the classical MCMC, the register $|x\rangle$ is initialized in an equiprobable superposition of all its states, effectively considering every state as a possible starting point.

The algorithm begins to applying a Hadamard gate (denoted H) to the action register $|a\rangle$, creating an equal superposition over all possible actions, thus enabling the walker to simultaneously consider all directions of movement. In the next step, as in the MCMC algorithm, a new trial is generated. This operation is performed using the TRIAL gate, which takes as input the registers $|a\rangle$ and $|x\rangle$, and places the resulting proposal in the output register $|t\rangle$.

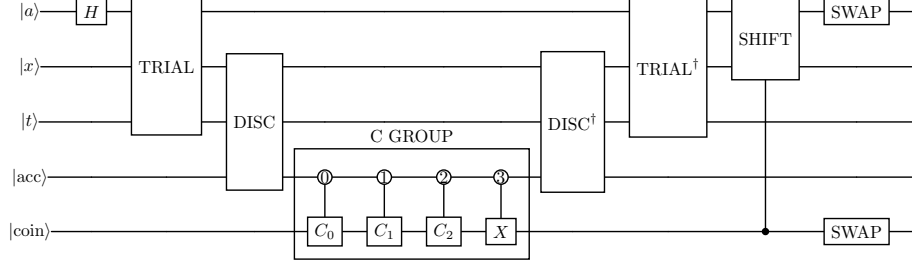


Fig. 3: Quantum circuit for the proposed QMCMC algorithm. The circuit is composed of four main operations: TRIAL, DISC, C GROUP (a collection of controlled C gates) and SHIFT. Gates marked with the symbol \dagger represent the inverses of their respective operations and are included to enable the reversibility and iteration of the process.

Consider a discrete space $\Sigma = \mathbb{Z}$, and actions defined by $\mathcal{A} = \{|0\rangle, |1\rangle\}$, the TRIAL gate behaves as follows: when $|a\rangle = |0\rangle$, it shifts the position leftward ($x_{\text{trial}} \leftarrow x - 1$), and when $|a\rangle = |1\rangle$, it shifts it rightward $x_{\text{trial}} \leftarrow x + 1$. This behavior is generalized in the definition of the TRIAL gate shown in Equation (7).

$$\text{TRIAL} = \sum_{a,x,t} |a, x, x - (-1)^a + t\rangle \langle a, x, t| \quad (7)$$

The second step involves calculating the acceptance probability A (as defined in Subsection 2.1, Equation (1)) and mapping it onto the quantum register $|acc\rangle$. Since quantum registers cannot natively represent continuous values, the interval $[0, 1]$ is discretized into a finite number of bins using a predefined discretization rule D . Each possible state of the register $|acc\rangle$ identifies one of these intervals, which will later determine the acceptance probability. Specifically, the discretization rule divides the range into $|\mathcal{H}_{\text{acc}}| - 1$ equally sized segments. The last value of $|acc\rangle$, corresponding to $|\mathcal{H}_{\text{acc}}|$, is reserved to represent acceptance probabilities equal to or exceeding 1. This mapping process is performed using the DISC gate, which acts on the quantum registers $|x\rangle$ and $|t\rangle$, assigning the correct identifier to $|acc\rangle$ as formalized in Equation (8).

$$\text{DISC} = \sum_{x,t,\text{acc}} |x, t, D + \text{acc}\rangle \langle x, t, \text{acc}|; \quad D(x, t) = \begin{cases} 0, & A(x, t) < 0.33 \\ 1, & 0.33 \leq A(x, t) < 0.66 \\ 2, & 0.66 \leq A(x, t) < 1 \\ 3, & A(x, t) \geq 1 \end{cases} \quad (8)$$

$$A(x, t) = \min\left(1, \frac{f(t)}{f(x)}\right)$$

Once the acceptance probability has been discretized, the quantum register $|acc\rangle$ is used as a control to activate the corresponding C_i gate on the quantum register $|coin\rangle$. This operation creates a superposition in $|coin\rangle$ that represents the acceptance probability associated with the proposal state in $|t\rangle$. In the implementation, the angles θ_i are preset to match the average value of each discretized interval, aiming to minimize rounding errors. It is important to highlight that the gate associated with the higher interval value is a NOT gate (X gate in quantum notation), as it only needs to flip the state of $|coin\rangle$ to $|1\rangle$. This discretization scheme allows for an increasingly accurate approximation of the continuous acceptance function as the size of $|acc\rangle$ grows, since more intervals can be represented.

Finally, once the quantum register $|coin\rangle$ encodes the probability of acceptance of the proposed state $|t\rangle$, the system updates its position within the state space. This update is controlled by the SHIFT gate, which operates on the registers $|a\rangle$, $|x\rangle$, and $|coin\rangle$. Specifically, the gate uses the value in $|coin\rangle$ to determine whether to perform the shift: if the proposal is accepted ($|coin\rangle = |1\rangle$), the register $|x\rangle$ is updated to reflect the new state; otherwise, it remains unchanged. The mathematical definition of the SHIFT gate is given in Equation (9).

$$\text{SHIFT} = \left(\sum_{a,x} |a, x\rangle \langle a, x| \right) \otimes |0\rangle \langle 0| + \left(\sum_{a,x} |a, x - (-1)^a\rangle \langle a, x| \right) \otimes |1\rangle \langle 1| \quad (9)$$

A key component of iterative quantum algorithms is the process known as uncomputation, which allows previously calculated values to be reversed and reset. This is essential for reusing quantum registers without disturbing the superposition states that may be entangled with other parts of the system. In the proposed circuit, uncomputation is applied to the registers $|t\rangle$ and $|acc\rangle$, returning them to the $|0\rangle$ state. Since all information required for the next iteration is encoded in the $|coin\rangle$ register, the inverse gates TRIAL^\dagger and DISC^\dagger are used to safely undo the previous operations.

However, the registers $|a\rangle$ and $|coin\rangle$ cannot be recomputed without disrupting the quantum state of $|x\rangle$, which now stores the computed probability distribution. Therefore, to support multiple iterations, these registers must be replaced with new ones initialized to $|0\rangle$. This is done using SWAP gates, which exchange the entangled registers with clean ones prepared for reuse. One limitation of this approach is that the number of qubits increases following the expression $2t + 2n_x + n_{acc}$, where n_x and n_{acc} are the sizes in qubits of $|x\rangle$ and $|acc\rangle$ registers respectively; setting a linear relation with the number of iteration.

4 Results

Before presenting and analyzing the results, three important points should be considered. First, the label that identifies each quantum state in the circuit does not directly correspond to its actual real-valued representation. In the experiments, the quantum state $|x\rangle = |0\rangle$ maps to the real value -5, and the state $|x\rangle = ||\mathcal{H}_x| - 1\rangle$ maps to 5. The intermediate values are derived via linear interpolation.

Second, note that the target function f is a continuous probability density function defined over an unbounded or very large domain. In order to represent it using a quantum register, the domain must be truncated to a finite interval, for example, $[-5, 5]$, and discretized into evenly spaced segments, each corresponding to a basis state of the quantum register $|x\rangle$. As a result, each state encodes the probability mass within a fixed-width subinterval. The discretized version of the target distribution, limited to the chosen interval, is referred to as the expected distribution, and it is this shape that the circuit aims to approximate. Importantly, while the resulting probability distribution always sums to 1, it only captures the structure of f within the truncated range.

Finally, the circuit was iterated until the resulting distribution converged. We understand that the circuit has converged when the distribution contained in the position register $|x\rangle$ in iteration t , which we denote as $U^t |x\rangle$, does not differ from the distribution obtained by applying one additional iteration. That is, when $U^t |x\rangle = U^{t+1} |x\rangle$. In each case, the value of t where the distribution no longer varies is used to evaluate the convergence rate of the circuit.

4.1 Analysis of the resulting distribution

Figure 4 presents 6 experiments performed using different parameters: (i) different target functions f , including single Gaussian distributions $G(\mu, \sigma)$ and mixtures of Gaussians, and (ii) varying sizes of the quantum register $|x\rangle$. In all cases, the size of the register $|\text{acc}\rangle$ was set equal to the size of $|x\rangle$, that is, $|\mathcal{H}_{\text{acc}}| = |\mathcal{H}_x|$. In Subfigure 4a, the circuit approximates $G(0; 1)$ and the resulting distribution closely matches the expected one in both the mean μ and the standard deviation σ . A similar result is seen in Subfigure 4b for $G(2; 1)$, where the distribution is shifted but also generates a good approximation. These results demonstrate that the circuit captures the structure of the target function f within the interval. However, due to the limited representational capacity of $|x\rangle$, the discretization of f becomes noticeable.

Increasing the size of the register $|x\rangle$, see Subfigures 4d and 4e, results in a more accurate approximation of the continuous function f . However, this improvement comes at the cost of a higher number of iterations required for convergence. This observation suggests a direct relationship between the size of $|x\rangle$ and the convergence speed: larger registers enable finer discretization but slow down the convergence.

In addition to the size of the register $|x\rangle$, the complexity of the function f is also a key factor to determine the number of iterations to reach convergence. Subfigures 4c and 4f, illustrating a mixture of Gaussians $G(0; 1) + G(3; 0.5)$, show a notable increase in the number of iterations needed. The last experiment (Subfigure 4f) is particularly insightful for two reasons: (i) it clearly demonstrates the significant impact of the complexity of f on convergence, and (ii) it reveals the circuit's decreasing convergence rate in the final iterations. While the initial evolution quickly approximates the expected distribution, progress slows considerably as the approximation improves. It's at this point that we stop the simulation and consider that the circuit has converged, avoiding looking for exactly the iteration t that satisfies $U^t |x\rangle = U^{t+1} |x\rangle$, which can be difficult due to possible numerical errors.

In general, the experiments confirm that the circuit successfully approximates the target distribution f effectively. However, the convergence rate remains a limiting factor. In all cases, the number of iterations required to achieve convergence far exceeds the number of states represented in $|x\rangle$, which suggests potential limitations in terms of scalability. Applying the circuit to more realistic problems with large and complex state spaces could be challenging, as it may require a significantly higher number of iterations.

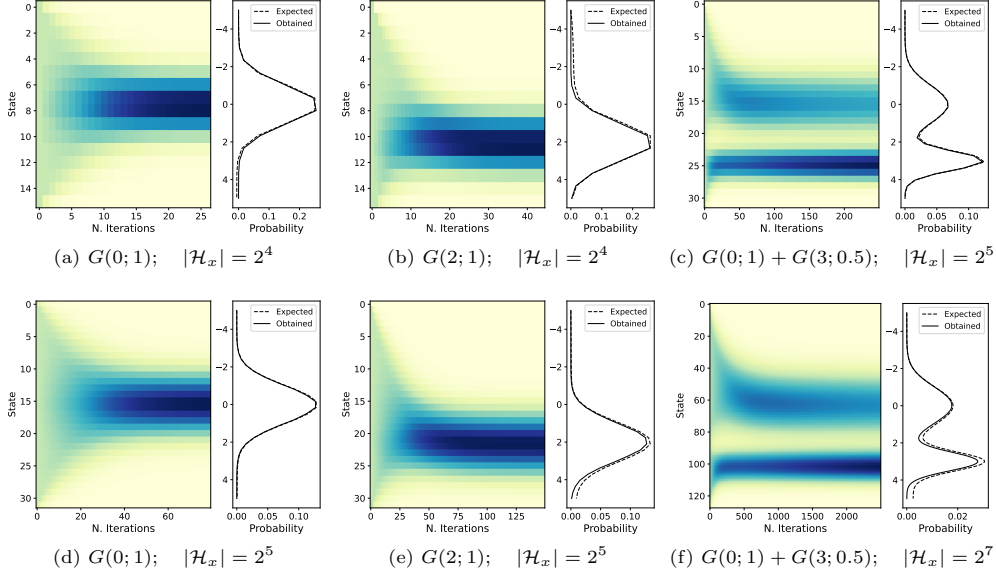


Fig. 4: The figure shows the results of several experiments evaluating the behavior of the circuit. Each subplot contains two visual elements: a heatmap that displays the evolution of the obtained distribution over iterations (columns), where yellow indicates less probable states and blue indicates more probable ones; and a line plot comparing the expected distribution (dashed line) with the distribution obtained from the circuit (solid line). It is observed how the circuit is able to adequately approximate the shape of the function f ; in our case, a set of gaussians and mixtures of gaussians. It is also observed how increasing the size of the register $|x\rangle$ allows for greater precision, at the cost of an increase in the number of iterations.

4.2 Effects of the qregister $|acc\rangle$

Another adjustable parameter in the circuit is the size of the quantum register $|acc\rangle$, which controls the discretization level of the acceptance probability (the “coin”). Experiments conducted with varying register sizes have shown that increasing this size

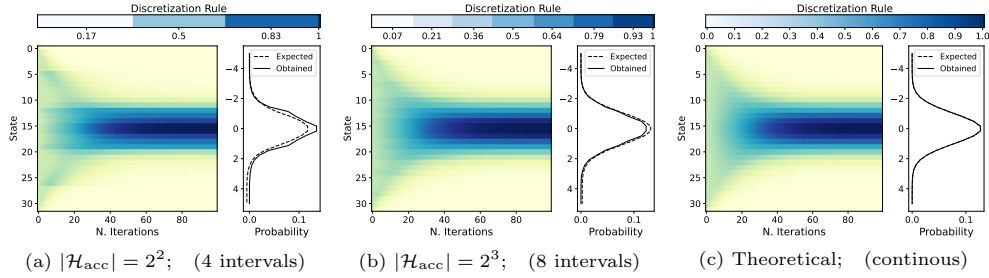


Fig. 5: The figure illustrates how the increase in size of $|a\rangle$ improves the quality of the approximation due to the greater number of intervals in the discretization rule; enabling better capturing the shape of f . In all subfigures, the target function f is a Gaussian distribution $G(0, 1)$.

improves the level of detail in the circuit’s approximation of the target distribution f . The results of these experiments are shown in Figure 5.

Subfigure 5c presents the theoretical scenario in which the acceptance probability of the coin is not discretized. Although such an operation cannot be implemented using unitary quantum gates in practice, simulation allows us to explore this idealized case. As expected, the resulting distribution closely follows a smooth form of the target f . When the discretization is introduced to make the gate unitary, some detail is lost, as shown in Subfigure 5a. However, as with the quantum register $|x\rangle$, increasing the size of $|acc\rangle$ improves the level of detail of the result (see Subfigure 5b). Furthermore, additional experiments confirm that larger register sizes consistently lead to better approximations of the target distribution.

All experiments in this section assume the discretization rule D defined in Equation (8), which uniformly divides the range $[0, 1)$ into equally sized, symmetrically distributed intervals. However, the method is not limited to this approach, alternative discretization schemes can be applied. Experiments conducted with different discretization strategies showed no significant variation in the behavior or quality of the resulting distributions.

The complexity of the function f plays an important role when choosing the size of the register $|acc\rangle$. Functions that exhibit high multimodality or abrupt trend changes, require finer discretization, i.e., more intervals, to capture their structure. As a general rule, setting the size of $|acc\rangle$ equal to that of $|x\rangle$ typically provides sufficient resolution for accurate representation. However, for simpler distributions, such as those shown in Subfigure 5b, a smaller quantum register may still obtain good approximation results.

4.3 Boosting convergence speed

As highlighted at the end of 4.1, and shown in Subfigure 4f, the circuit exhibits a slow convergence rate, requiring a number of iterations t significantly greater than the number of representable states in the register $|x\rangle$. This effect is particularly noticeable in that case, but similar behavior is observed across all evaluated configurations. This

limitation reduces the applicability of the circuit in real-world scenarios, where the state space is typically large. Therefore, reducing the number of iterations—that is, increasing the convergence speed—is crucial to improving the usability of the proposed method. To address this, we modify the register $|a\rangle$ to allow for a larger set of possible moves within a single iteration.

As described in Section 3, the original circuit allows each position to move only to its immediately adjacent states. This constraint mirrors the behavior of classical MCMC algorithms, where each proposed move requires evaluating the function f , typically at a high computational cost. However, in the quantum setting, this limitation can be relaxed: superposition enables simultaneous evaluation of f at multiple positions, as already exploited by the register $|a\rangle$. By increasing the size of $|a\rangle$, we can encode a wider set of candidate moves and explore the state space more broadly in each iteration.

With this modification, the circuit is capable of evaluating up to $|\mathcal{H}_a| = |\mathcal{H}_x|/2$ proposals per iteration. Equation (10) defines the updated TRIAL and SHIFT gates that implement this extended behavior; where the indicator function $\mathbf{1}_{\{a \geq \frac{|\mathcal{H}_a|}{2}\}}$ avoids movement from any $|a\rangle$ to itself. Ideally, one would allow unrestricted movement across the entire state space—i.e., setting $\mathcal{H}_a = \mathcal{H}_x$. However, we have not identified a unitary operation that achieves this, at least within the architectural constraints of the circuit shown in Figure 3.

$$\begin{aligned} \text{TRIAL} &= \sum_{a,x,t} \left| a, x, x + a + \mathbf{1}_{\{a \geq \frac{|\mathcal{H}_a|}{2}\}} - \frac{|\mathcal{H}_a|}{2} + t \right\rangle \langle a, x, t| \\ \text{SHIFT} &= \left(\sum_{a,x} |a, x\rangle \langle a, x| \right) \otimes |0\rangle \langle 0| + \\ &\quad \left(\sum_{a,x} \left| a, x + a + \mathbf{1}_{\{a \geq \frac{|\mathcal{H}_a|}{2}\}} - \frac{|\mathcal{H}_a|}{2} \right\rangle \langle a, x| \right) \otimes |1\rangle \langle 1| \end{aligned} \quad (10)$$

Figure 6 presents a set of experiments conducted to analyze the effect of the register size $|a\rangle$ on the convergence behavior of the circuit. In all simulations, the target function f was a mixture of Gaussians of the form $G(-3, 1) + G(3, 1)$, and the position register $|x\rangle$ was configured with 5 qubits. In Subfigure 6a, the baseline configuration is shown, with $|\mathcal{H}_a| = 2^1$, where the previously discussed behavior is evident: the number of iterations required for convergence exceeds twice the number of available states in $|x\rangle$. When the size of $|a\rangle$ is increased by one qubit (Subfigure 6b), the required number of iterations is reduced by nearly half. This outcome aligns with expectations, as each additional qubit doubles the number of available candidate moves.

Finally, in Subfigure 6c, where the register $|a\rangle$ reaches its maximum size for $|\mathcal{H}_x| = 2^5$, convergence is achieved with fewer iterations than the number of possible states in $|x\rangle$. Notably, this reduction in the number of required iterations, below the cardinality of the state space, has been consistently observed, independently of the choice of

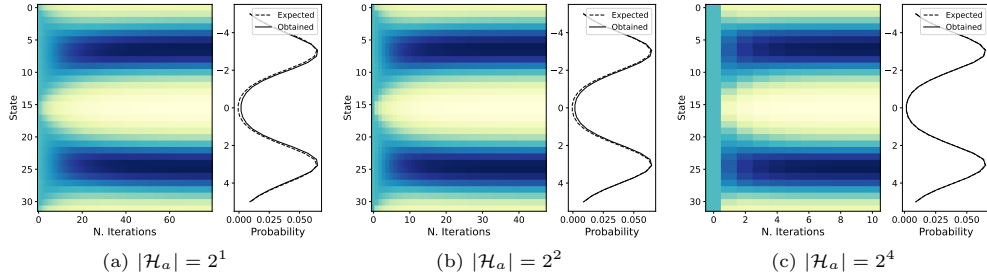


Fig. 6: The figure shows the results obtained from simulations performed with increasing sizes of the register $|a\rangle$, allowing more movements per iteration when sampling from the mixture of Gaussians $G(-3, 1) + G(3, 1)$. The subfigures show the reduction in the number of iterations required to reach convergence as the size of $|a\rangle$ increases.

function f and the size of $|x\rangle$. This improvement is therefore not limited to the specific case presented in Figure 6.

While the reduction in the number of iterations is significant, it comes at the expense of increased computational resource usage. As discussed in Section 3, the register $|a\rangle$ is replaced in each iteration, which means that increasing its size directly multiplies the total number of qubits required by the circuit. This effect is quantified in Equation (11), where n_a denotes the number of qubits in $|a\rangle$.

At this point, it is natural to question whether the gain in convergence speed justifies the additional qubit cost, especially in the context of current quantum hardware limitations. For instance, in the simulations shown in Subfigures 6a and 6c, and based on Equation (11), we find that the first simulation requires 175 qubits³ to reach convergence after 80 iterations. In contrast, the second simulation, using a larger $|a\rangle$ register, requires only 65 qubits, amounting to a 68% reduction. This behavior has been consistently observed in multiple experiments, with the reduction becoming more pronounced as the size of the register $|x\rangle$ increases.

$$(n_a + 1)t + 2n_x + n_{acc} \quad (11)$$

5 Conclusions

In this work, we have proposed a quantum version of the MCMC algorithm based on a quantum walk circuit architecture. The target distribution is encoded in the superposition of states of the position register $|x\rangle$, exploiting the quantum walk's accelerated exploration of the state space to improve sampling efficiency.

The results demonstrate that the circuit successfully captures the structure of the target distribution f , effectively emulating the behavior of the classical MCMC

³This count includes only the logical qubits forming the registers discussed; ancillary qubits required for circuit implementation are not considered.

algorithm described in Subsection 2.1. Furthermore, we introduced a modification that enables the evaluation of multiple candidate moves per iteration. This enhancement not only accelerates convergence but also reduces the number of required qubits by decreasing the total number of iterations.

As observed in Subsection 4.1, the quality of the approximation to f is sensitive to the discretization of the acceptance probability, which depends on the size of the register $|\text{acc}\rangle$. In most experiments, we adopted the configuration $|\mathcal{H}_{\text{acc}}| = |\mathcal{H}_x|$, which generally yields accurate approximations. However, as shown in Subfigure 4f, the approximation quality also depends on the complexity of f . Deriving an analytical expression that relates the approximation error to the sizes of $|x\rangle$ and $|\text{acc}\rangle$, and to the structure of f , would be of great value.

Another important consideration is the number of iterations required to reach convergence. In our simulations, convergence was assumed when the distribution encoded in $|x\rangle$ remained effectively unchanged across successive iterations. However, this stopping condition relies on privileged information that is not available in realistic scenarios. As with the approximation error, it would be useful to develop a formal bound or predictive expression for the number of iterations required to achieve convergence.

These observations suggest several directions for future work. (i) Investigate the relationship between the function f and the size of the acceptance register $|\text{acc}\rangle$, with the aim of deriving a predictive model for approximation accuracy. (ii) Analyze the dependency between f and the size of the position register $|x\rangle$ to estimate convergence time. (iii) Explore practical implementation of the algorithm on real quantum hardware, focusing on reducing abstraction, building a compilable version, and studying its behavior under noisy conditions typical of NISQ-era devices.

Acknowledgements. This research is supported by the Basque Government through IKUR-HPC-IA-Materiales Avanzados grant and projects IT1504-22, KK-2023/00012, KK-2023/00090, KK-2024/00030 and KK-2024/00068. It is also supported by the grant PID2023-152390NB-I00 and CNS2023-144315 funded by MICIU/AEI/10.13039/9/501100011033, “European Union NextGenerationEU/PRTR” and by “FEDER funds”. Dr. Javier Navaridas holds a Ramon y Cajal fellowship funded by the Spanish Ministry of Science, Innovation and Universities (RYC2018-024829-I), MCIN/AEI/10.13039/501100011033 and, as appropriate, by “ESF Investing in your future” or by “EU NextGenerationEU/PRTR”.

Declarations

- Funding
The funding is specified in above Acknowledgements section.
- Conflict of interest
The authors did not receive support from any organization that may gain or lose financially through publication of this manuscript.
- Ethics approval and consent to participate (Not applicable)
- Consent for publication (Not applicable)
- Data availability (Not applicable)

- Materials availability (Not applicable)
- Code availability
The code is available from the corresponding author on reasonable request.
- Author contribution
All authors contributed to the study conception and design.

References

- [1] Frenkel, D., Smit, B.: Understanding Molecular Simulation: From Algorithms to Applications, 1st edn. Academic Press, Inc., USA (1996)
- [2] Metropolis, N., Rosenbluth, A.W., al.: Equation of state calculations by fast computing machines. *The Journal of Chemical Physics* **21**(6), 1087–1092 (1953) <https://doi.org/10.1063/1.1699114>
- [3] Hastings, W.K.: Monte carlo sampling methods using markov chains and their applications. *Biometrika* **57**(1), 97–109 (1970) <https://doi.org/10.1093/biomet/57.1.97>
- [4] Nielsen, M.A., Chuang, I.L.: Quantum Computation and Quantum Information, 10th anniversary edition edn. Cambridge University Press, UK (2000)
- [5] Preskill, J.: Quantum computing in the NISQ era and beyond. *Quantum* **2**, 79 (2018) <https://doi.org/10.22331/q-2018-08-06-79>
- [6] Aharonov, Y., Davidovich, L., Zagury, N.: Quantum random walks. *Phys. Rev. A* **48**, 1687–1690 (1993) <https://doi.org/10.1103/PhysRevA.48.1687>
- [7] Ambainis, A.: Quantum walk algorithm for element distinctness. *SIAM J. Comput.* **37**(1), 210–239 (2007) <https://doi.org/10.1137/S0097539705447311>
- [8] Szegedy, M.: Quantum speed-up of markov chain based algorithms. In: 45th Annual IEEE Symposium on Foundations of Computer Science, pp. 32–41 (2004). <https://doi.org/10.1109/FOCS.2004.53>
- [9] Childs, A.M., Goldstone, J.: Spatial search by quantum walk. *Phys. Rev. A* **70**, 022314 (2004) <https://doi.org/10.1103/PhysRevA.70.022314>
- [10] Ambainis, A.: Quantum walks and their algorithmic applications. *International Journal of Quantum Information* **01**(04), 507–518 (2003) <https://doi.org/10.1142/S0219749903000383>
- [11] Childs, A.M.: Universal computation by quantum walk. *Phys. Rev. Lett.* **102**, 180501 (2009) <https://doi.org/10.1103/PhysRevLett.102.180501>
- [12] Zähringer, F., Kirchmair, G., al.: Realization of a quantum walk with one and two trapped ions. *Phys. Rev. Lett.* **104**, 100503 (2010) <https://doi.org/10.1103/>

- [13] Schreiber, A., Gábris, A., al: A 2d quantum walk simulation of two-particle dynamics. *Science* **336**(6077), 55–58 (2012) <https://doi.org/10.1126/science.1218448>
- [14] Peruzzo, A., Lobino, M., al.: Quantum walks of correlated photons. *Science* **329**(5998), 1500–1503 (2010) <https://doi.org/10.1126/science.1193515>
- [15] Geman, S., Geman, D.: Stochastic relaxation, gibbs distributions, and the bayesian restoration of images. *IEEE Transactions on Pattern Analysis and Machine Intelligence* **PAMI-6**(6), 721–741 (1984) <https://doi.org/10.1109/TPAMI.1984.4767596>
- [16] Earl, D.J., Deem, M.W.: Parallel tempering: Theory, applications, and new perspectives. *Phys. Chem. Chem. Phys.* **7**, 3910–3916 (2005) <https://doi.org/10.1039/B509983H>
- [17] Miasojedow, B., Moulines, E., Vihola, M.: An adaptive parallel tempering algorithm. *Journal of Computational and Graphical Statistics* **22**(3), 649–664 (2013) <https://doi.org/10.1080/10618600.2013.778779>